DOI: 10.1002/cphc.201200224

DNA Photocleavage by a Cationic BODIPY Dye through Both Singlet Oxygen and Hydroxyl Radical: New Insight into the Photodynamic Mechanism of BODIPYs

Jianguang Wang,[a, b] Yuanjun Hou,[a] Wanhua Lei,[a] Qianxiong Zhou,[a] Chao Li,[a] Baowen Zhang,[a] and Xuesong Wang*[a]

Two new NIR-absorbing BODIPY dyes, each bearing two pyridinium groups, are synthesized and their DNA-binding affinities and DNA photocleavage abilities examined in depth. While one BODIPY dye photocleaves DNA mainly through singlet oxygen, the other photocleaves DNA through both singlet oxygen and hydroxyl radical. To the best of our knowledge, this is the first example of a hydroxyl radical being involved in the photodynamic behavior of BODIPY-type dyes. EPR experiments confirm the ability of these and several related BODIPYs to generate superoxide anion radical and hydroxyl radical. This finding may shed light on the mechanism of BODIPY-based photodynamic therapy (PDT) and open a new avenue for development of more efficient BODIPY-type PDT agents.

1. Introduction

Photodynamic therapy (PDT) is a minimally invasive treatment for a variety of cancers by interaction of three elements: light, a photosensitizer, and oxygen. When exposed to proper wavelengths of light, the photosensitizer can be activated and undergo electron/energy transfer through its triplet excited state to generate cytotoxic reactive oxygen species (ROS), mainly singlet oxygen ($^1O_2$).[1] Although several porphyrin photosensitizers, for example, Photofrin, are approved for clinical treatment of certain types of cancers, they are far from ideal. One of the main drawbacks of these photosensitizers is the relatively weak absorbance in the phototherapeutic window of 600–900 nm. For Photofrin, the drawbacks also include the complicated components from which it is composed and long-term skin photosensitivity after PDT.[2] Such limitations encourage great efforts to search for new and more effective photosensitizers, including porphyrin-type photosensitizers such as chlorin and bacteriochlorin,[3] and non-porphyrin-type photosensitizers such as cyanine dyes, squaraines, and boradiazaindacenes (abbreviated hereafter as BODIPY).[2e,4]

The BODIPYs are versatile organic dyes which have found wide applications in biological labeling and imaging,[5] luminescent devices,[5] chemical sensors,[5,6] solar cells,[7] and photocatalytic hydrogen generation,[8] due to their excellent thermal and photochemical stability, high fluorescence quantum yield, intense absorption profile, good solubility, and chemical robustness. The intense absorption of BODIPYs in the near-infrared (NIR) region makes them suitable for PDT application, but the low intersystem crossing (ISC) efficiency severely hampers the ability to generate $^1O_2$ and thus the photodynamic activity of BODIPYs. In 2002, O'Shea and co-workers successfully dealt with this problem by introduction of bromine atoms into a series of aza-BODIPYs to give the resulting dyes high $^1O_2$ quantum yields and potent photodynamic activity.[9] Recently, Ramaiah and co-workers improved the $^1O_2$ quantum yields of aza-BODIPYs further by attaching four iodine atoms on the dye skeleton.[10] In 2005, Nagano et al. disclosed that an iodinated BODIPY is also a good $^1O_2$ photosensitizer, but the examined dye suffers from short absorption wavelength.[11] Akkaya et al. extended the absorption bands of brominated or iodinated BODIPYs into the phototherapeutic window by incorporating conjugation structures at 3- and 5-positions of the BODIPY core.[12] Recently, Ng and co-workers also reported a series of unsymmetrical distyryl iodinated BODIPYs that show high in vitro PDT activities.[13] Additionally, You and co-workers found that fusion of brominated thiophene rings with the BODIPY core may improve $^1O_2$ quantum yield remarkably.[14] While much interest focused on the $^1O_2$ efficiency, absorption window, and water solubility of the BODIPY family, another important factor, that is, the bioavailability of $^1O_2$, should also be paid proper attention. $^1O_2$ is a highly reactive species but has a short apparent lifetime (ca. 2.0 μs), a low apparent diffusion coefficient (4×10^{-6} cm^2 s), and thus a very limited sphere of activity (about 155 nm in radius) in biological systems, and this implies the importance of the binding ability of PDT agents

[a] Dr. J. G. Wang, Prof. Y. J. Hou, Dr. W. H. Lei, Dr. Q. X. Zhou, Dr. C. Li, Prof. B. W. Zhang, Prof. X. S. Wang
Key Laboratory of Photochemical Conversion and Optoelectronic Materials
Technical Institute of Physics and Chemistry
Chinese Academy of Sciences
Beijing 100190 (China)
Fax: (+86) 10-6487-9375
E-mail: g203@mail.ipc.ac.cn
xswang@mail.ipc.ac.cn

[b] Dr. J. G. Wang
Graduate University of Chinese Academy of Sciences
Beijing 100049 (China)

Supporting information for this article is available on the WWW under http://dx.doi.org/10.1002/cphc.201200224.

toward their biotarget.[15] DNA is one of the main targets of many anticancer drugs, including PDT agents.[16] As a result, DNA photocleavers, particularly activated by visible and NIR light, are highly pursued due to their promising potential in PDT. Owing to the negatively charged character of DNA, a variety of positively charged dye molecules were scrutinized as DNA photocleavers to take advantage of the attractive electrostatic interaction, which may enhance the binding affinity of the dye molecules toward DNA and therefore improve the bioavailability of the ROS.[17] Though several BODIPYs or aza-BODIPYs bearing either quaternary ammonium groups or protonatable pyridyl groups were investigated as potential PDT agents,[9d,12d,13b,18] there are no reports on the interactions of cationic BODIPYs and DNA up to now, which is believed to be helpful for better understanding of their PDT mechanism.

In this work, two BODIPY dyes **6** and **7** bearing pyridinium groups (Scheme 1) were synthesized and their binding features and photocleavage activities toward DNA were examined in depth. Unexpectedly, while **7** photocleaves DNA exclusively through $^1O_2$, **6** photocleaves DNA through both $^1O_2$ and hydroxyl radical (•OH). Further experiments indicate that **1**, **2**, and **3** can also generate •OH with different efficiencies. To the best of our knowledge, this is the first example that BODIPYs are able to generate •OH on visible and NIR irradiation. Since •OH is the most active among all ROS, these results may open a new avenue for the development of novel and more efficient BODIPY-based PDT agents

2. Results and Discussion

2.1. Synthesis, Photophysical, and Photochemical Properties

The BODIPY **1** was synthesized by following reported procedures.[6a] Bromination or iodination of **1** led to formation of BODIPY **2** or **3**, which, after further condensation with 4-pyridinecarboxaldehyde, transformed into BODIPY **4** or **5**, respectively. By reaction with iodomethane, target BODIPYs **6** and **7** were finally obtained, as shown in Scheme 1. Both **6** and **7** were structurally identified by ^{1}H NMR and HRMS. For comparison, **1**–**5** were also isolated and structurally characterized by ^{1}H NMR and EI-MS or MALDI-TOF MS.

Figure 1a shows the visible absorption spectra of **1**–**7** in acetonitrile. Compared to **1**, bromination or iodination at 2- and 6-positions of **1** leads to about 25 nm (for **2**) and 31 nm (for **3**) redshift in absorption maxima (Table 1). Further conjugation with pyridyl-substituted ethylene at 3- and 5-positions gives rise to another 100 nm of bathochromic shift. Finally, methylation at pyridyl N atoms makes the visible absorption bands of **6** and **7** totally move into the phototherapeutic window, with absorption maxima centered at 648 and 649 nm, respectively. Moreover, the molar extinction coefficients of **6** and **7** at their absorption maxima are 4.5×10^4 cm^{-1} M^{-1} and 5.6×10^4 cm^{-1} M^{-1}, respectively, much larger than that of the Q bands of general porphyrin-based photosensitizers.

Similar to the absorption spectra, the fluorescence emission spectra also experience a marked redshift from **1**, over **2**–**5**, to **6** and **7**, as shown in Figure 1b and Table 1. As expected, the fluorescence quantum yields of **2** and **3** decrease significantly with respect to **1**, mainly due to the intramolecular heavy-atom effect of bromine or iodine atoms. For **6** and **7**, the fluorescence quantum yields decrease further than for **2** and **3**, which may be attributed to intramolecular charge transfer (ICT) rather than energy-gap law, since **2** and **4** or **3** and **5** have similar fluorescence quantum yields

We also measured the oil/water partition coefficients of **6** and **7**. Due to the presence of two pyridinium groups, both **6** and **7** display amphiphilic char-

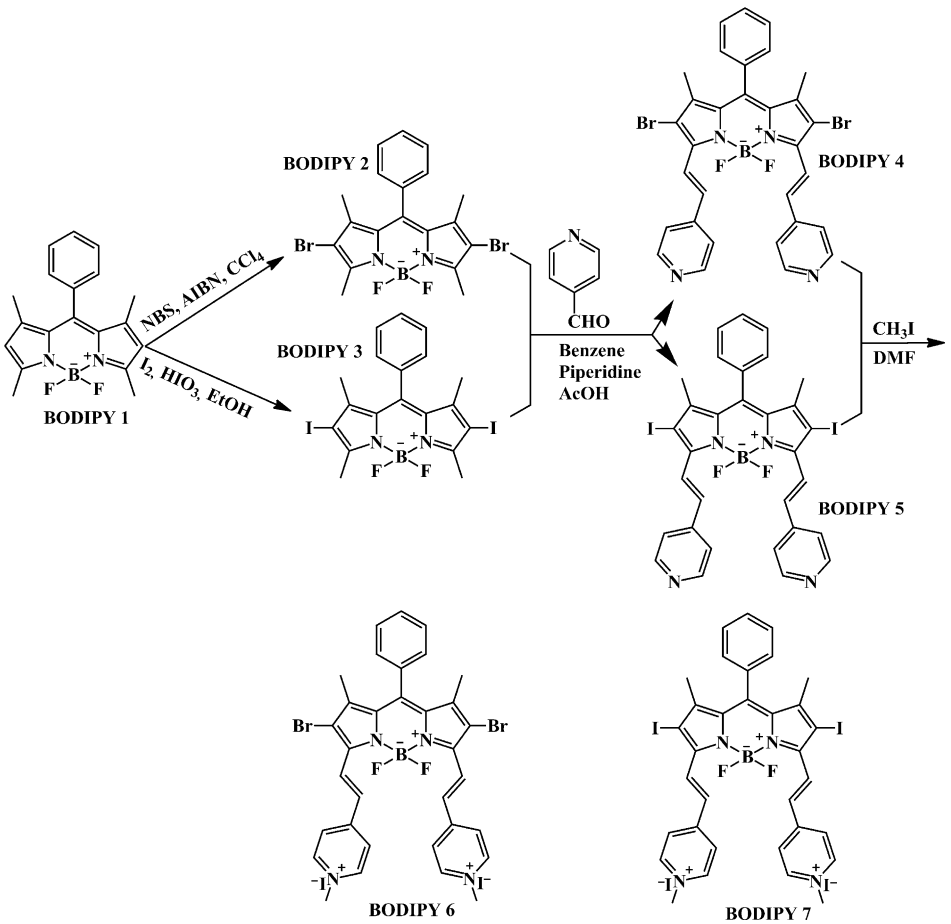

Scheme 1. Synthesis of the examined BODIPY dyes.

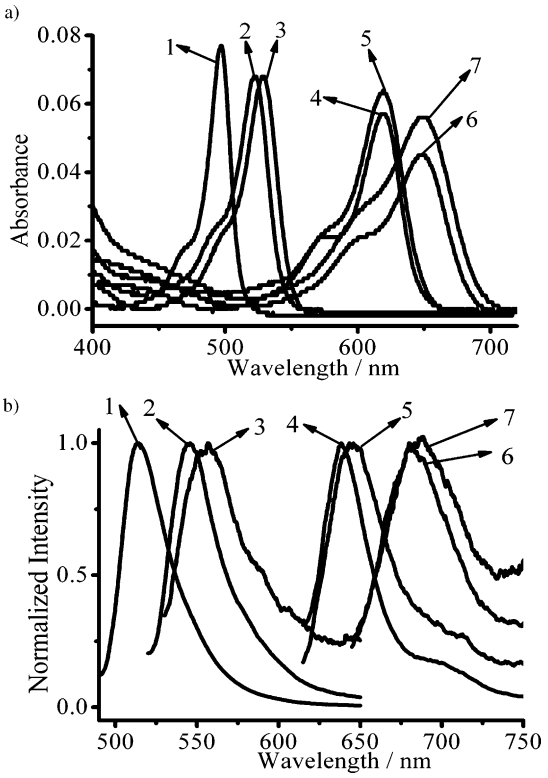

Figure 1. Visible absorption (a) and normalized fluorescence emission (b) spectra of **1**–**7** (1.0 μM) in acetonitrile.

Table 1. Photophysical properties of BODIPYs **1**–**7**.

Compound	λ_{abs}(max) [nm][a]	ε (cm^{-1} M^{-1})[a]	λ_{em}(max) [nm][a]	Φ_{fl}	Φ_{Δ}[d]	P_c[e]
1	497	77000	514	0.71[b]	n.d.[f]	n.d.
2	522	68000	544	0.18[b]	n.d.	n.d.
3	528	68000	556	0.032[b]	n.d.	n.d.
4	620	57000	638	0.19[c]	n.d.	n.d.
5	620	64000	643	0.04[c]	n.d.	n.d.
6	648	45000	680	0.095[c]	0.10	0.29
7	649	56000	686	0.014[c]	0.22	0.34

[a] Absorption maxima, molar extinction coefficients at absorption maxima, and fluorescence maxima measured in acetonitrile. [b] Fluorescence quantum yields determined at 25 °C by using fluorescein in 0.1 M aqueous NaOH solution as standard ($\Phi_{fl}=0.85$[19]). [c] Fluorescence quantum yields determined at 25 °C by using MB in ethanol as standard ($\Phi_{fl}=0.04$[20]). [d] Singlet oxygen quantum yields determined by the AMDA bleaching method, taking MB in PBS buffer as reference ($\Phi_{\Delta}=0.52$[33]). [e] *n*-Octanol/water partition coefficients. [f] n.d.: not determined.

acter, with *n*-octanol/water partition coefficients of 0.29 and 0.34, respectively. Amphiphilicity is expected to be an advantage for PDT agents by simplifying formulation and favoring cellular internalization.[21]

The $^1O_2$ generation efficiencies of **6** and **7** in aqueous solutions were evaluated by the AMDA bleaching method.[22] On irradiation with light above 600 nm, the absorbance of AMDA at 400 nm decreased gradually in the presence of **6** or **7** as a result of its reaction with generated $^1O_2$ (Figure 2). In contrast, no absorbance decrease was observed in the absence of **6** and **7**, that is, $^1O_2$ stems from the excited **6** or **7**. With MB as reference, the $^1O_2$ quantum yields of **6** and **7** are estimated to be 0.10 and 0.22, respectively, in good agreement with the stronger heavy-atom effect of iodine compared to bromine.

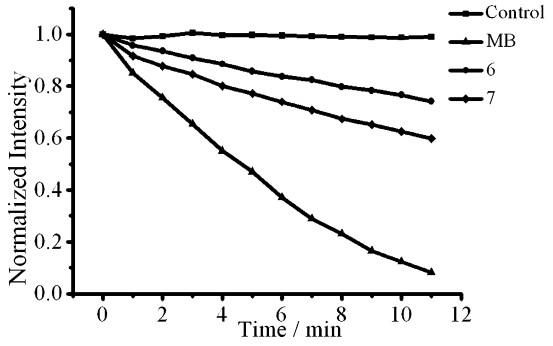

Figure 2. Time-dependent photobleaching of AMDA sensitized by **6**, **7**, or MB in PBS. The absorbance changes of AMDA at 400 nm were monitored as a function of irradiation ($\lambda > 600$ nm) time. A control experiment was carried out in the absence of photosensitizer.

The ability of **6** and **7** to generate $^1O_2$ was also confirmed by EPR experiments. As shown in Figure 3, irradiation of an air-saturated CH_3CN solution of **6** or **7** and TEMP with a 532 nm laser led to a three-line EPR spectrum with equal intensity and hyperfine coupling constants of $\alpha^N = 16.0$ G, which is assignable to TEMPO (the adduct of TEMP and $^1O_2$).[23] The TEMPO signal intensity of **7** is larger than that of **6**, in line with the AMDA bleaching experiments. Additionally, we also compared the TEMPO signal intensities of **1**–**5** as shown in Figure S1 (Supporting Information). The $^1O_2$ generation efficiencies follow the order **1** < **2** < **3** and **4** < **5**, in accordance with the heavy-atom effect.

2.2. DNA Binding Properties

Before examining the DNA photocleavage activities of **6** and **7**, their binding toward CT DNA was first studied by absorption titration, circular dichroism spectroscopy, viscosity experiments, and EB displacement assay.

Absorption titration is one of the simplest and most useful methods to investigate the binding interactions of small molecules, particularly dyes, toward DNA. Figure 4 shows the absorption spectral changes of **7** on titration of CT DNA. At the beginning of titration ($0 \le R \le 1.5$, R = [CT DNA]/[**7**]), significant hypochromism (42% at $R = 1.5$ vs. $R = 0$) and a bathochromic shift around 670–750 nm were observed. Further addition of CT DNA ($1.5 \le R \le 6$), however, led to a hyperchromic effect (43% at $R = 3$ vs. $R = 1.5$) and a hypsochromic shift around 600–700 nm. At $R > 6$, the absorption band of **7** shows hypochromism and bathochromic shift again. Titration of **6** by CT DNA gave similar results (Figure S2, Supporting Information). Though the spectral changes are somewhat complex, particu-

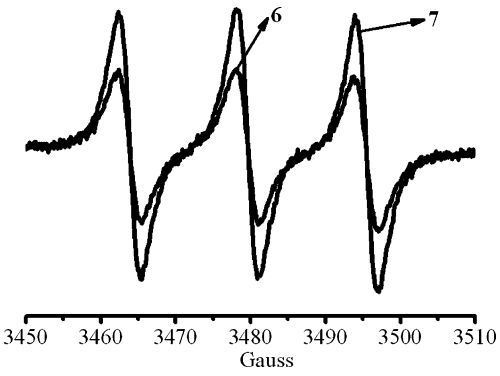

Figure 3. EPR signals obtained on irradiation of air-saturated CH_3CN solutions of TEMP (50 mM) and **6** or **7** (1 mM) with a 532 nm laser.

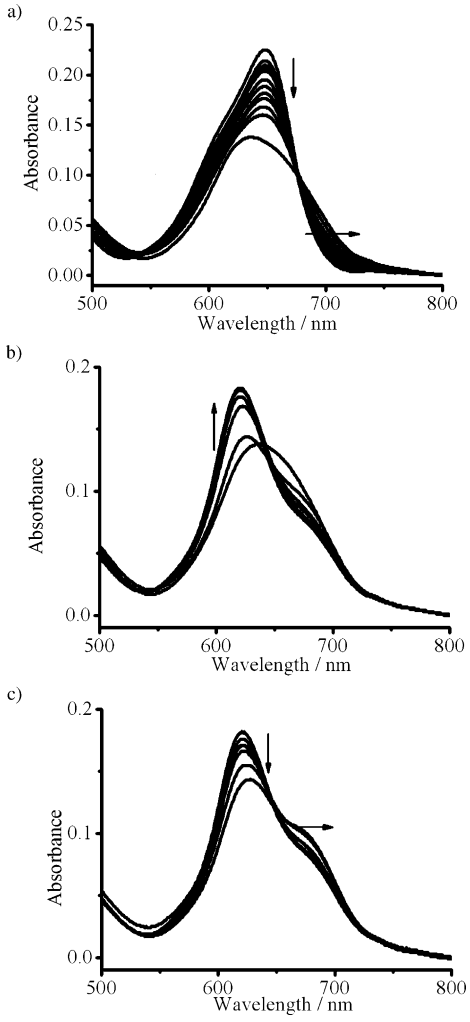

Figure 4. Absorption spectral changes of **7** (5 μM) on titration of CT DNA (0–0.1 mM) in PBS buffer (pH 7.4). a) $0 \le R \le 1.5$, b) $1.5 \le R \le 6$ and c) $6 \le R \le 20$ (R = [CT DNA]/[**7**]).

larly at $1.5 \le R \le 6$, the overall trends are hypochromism and bathochromic shift. Such spectral responses suggest an intercalation binding mode between CT DNA and **6** or **7**. Intercalation leads to a strong coupling between the π* orbital of the ligand and the π orbitals of the DNA base pairs, and thus decreases the π–π* transition energy of the ligand and results in a bathochromic shift. On the other hand, the coupling π* orbital is partially filled by electrons, and thus decreases the transition probabilities and leads to hypochromism.[24]

Circular dichroism measurements provide more information on the binding interactions of **6** and **7** toward CT DNA. As shown in Figure 5 and Figure S3 (Supporting Information), no CD signals can be detected within the range of 550–750 nm

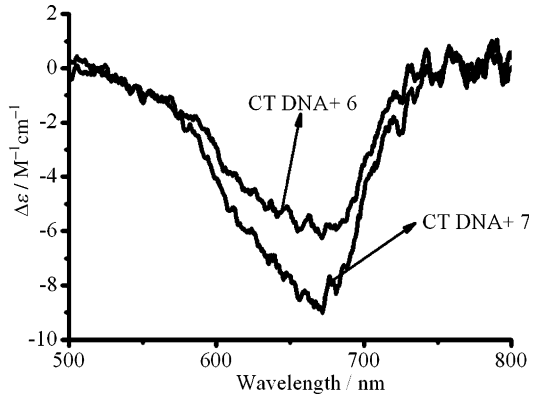

Figure 5. ICD spectra of **6** and **7** (10 μM) in the presence of CT DNA (50 μM).

for PBS solutions of **6** and **7**. However, the presence of CT DNA results in a negative CD signal within the absorption bands of **6** and **7**, which indicates a ligand–DNA interaction. Intercalators usually exhibit small induced CD (ICD) signals, $< 10\ M^{-1}cm^{-1}$ at the maximum of the ICD signal, although the magnitude of the signal does depend on the oscillator strength of the ligand transitions.[25] In our case, $\Delta\varepsilon$ values are $-5.96\ M^{-1}cm^{-1}$ for **6** and $-8.25\ M^{-1}cm^{-1}$ for **7**, in good agreement with the intercalation binding mode.

More convincing evidence for the intercalation of **6** and **7** with CT DNA comes from viscosity experiments. Intercalators such as EB generally cause a remarkable specific viscosity enhancement of DNA, as the result of the elongation of the DNA helix caused by insertion of planar aromatic chromophores between base pairs.[26] As shown in Figure 6, both **6** and **7** can in-

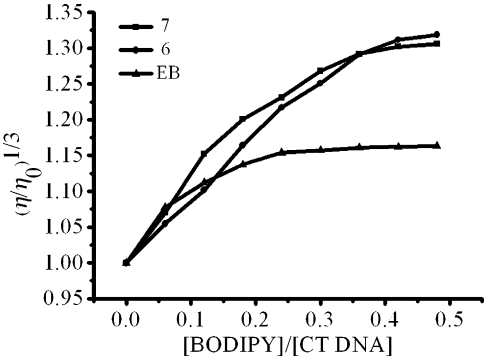

Figure 6. Relative specific viscosities of CT DNA at 30.0 °C in 5 mM PBS (pH 7.2) as a function of the concentration ratio of photosensitizer and CT DNA ([CT DNA] = 165 μM, [**6** or **7**] = 0–80 μM).

crease the specific viscosity of CT DNA more efficiently than EB, and this confirms their intercalation binding toward DNA.

An EB displacement assay was carried out to determine the apparent binding constants K_{app} of **6** and **7** to CT DNA. On addition of **6** or **7** (Figure 7) to the EB/CT DNA solution, the EB fluorescence was quenched effectively due to its displacement

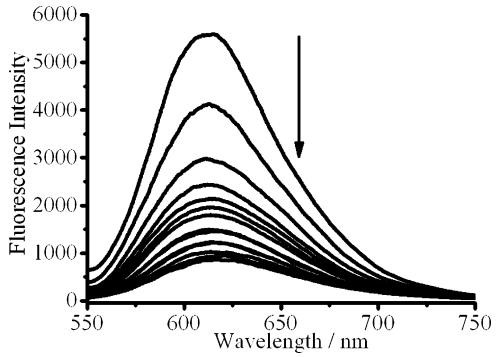

Figure 7. Fluorescence quenching of the EB (5 μM)–CT DNA (10 μM) solution in PBS by **7** (0–2.5 μM). The arrow indicates increasing concentration of **7**.

from DNA by **6** or **7**, from which K_{app} of $5.7\times10^7\,M^{-1}$ for **6** and $9.8\times10^7\,M^{-1}$ for **7** can be obtained. We also measured the binding constant of MB, a well known intercalator,[27] under the same conditions. The higher affinities of **6** and **7** toward CT DNA compared EB ($K_{app}=1.0\times10^7\,M^{-1}$)[35] and MB ($K_{app}=2.7\times10^7\,M^{-1}$) can at least partly ascribed to their two positive charges.

2.3. DNA Photocleavage

The DNA photocleavage activities of **6** and **7** were characterized by using pBR322 plasmid DNA as target. On NIR irradiation ($\geq$600 nm), both **6** and **7** can lead to DNA cleavage from supercoiled circular form to nicked circular form (Figure 8). Control experiments show that irradiation and the presence of **6** or **7** are necessary for DNA cleavage. The higher photocleavage activity of **7** compared to **6** can be attributed to its higher DNA affinity and larger $^1O_2$ quantum yield. We also examined the DNA photocleavage activity of MB under the same conditions (Figure S4, Supporting Information). The cleavage activities follow the order **7** > MB > **6**. The fact that MB sensitizes $^1O_2$

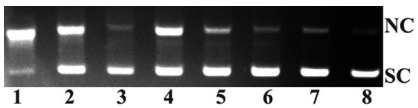

Figure 8. Comparison of agarose gel electrophoresis patterns of photocleaved supercoiled pBR322 DNA (0.1 mM in base pairs) by **6** and **7** (30 μM) in Tris/CH_3COOH/EDTA buffer (pH 7.4). Lane 1: DNA + **7** (50 min irradiation); lane 2: DNA + **7** (25 min irradiation); lane 3: DNA + **7** (in dark); lane 4: DNA + **6** (50 min irradiation); lane 5: DNA + **6** (25 min irradiation); lane 6: DNA + **6** (in dark); lane 7: DNA alone (50 min irradiation); lane 8: DNA alone (in dark). SC and NC denote supercoiled circular and nicked circular form, respectively.

generation more efficiently than **7** allows one to recognize the key role of DNA affinity, which can improve the bioavailability of $^1O_2$ and compensate the low $^1O_2$ quantum yield.

To examine the photodynamic mechanisms behind the DNA photocleavage, a series of ROS scavengers, including NaN_3 for $^1O_2$,[28] SOD and catalase for superoxide anion radical ($O_2^{\cdot-}$),[29] and KI for $^{\cdot}OH$,[30] were utilized to modulate the photocleavage activities of **6** and **7**. As shown in Figure 9, only NaN_3 inhibits

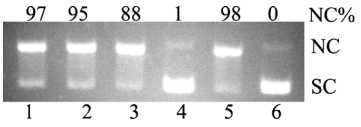

Figure 9. Comparison of agarose gel electrophoresis patterns of photocleaved supercoiled pBR322 DNA (0.1 mM in base pairs) by **7** (30 μM) in Tris/CH_3COOH/EDTA buffer (pH 7.4). Lane 1: DNA + **7** + catalase (0.05 mM); lane 2: DNA + **7** + SOD (500 U mL^{-1}); lane 3: DNA + **7** + KI (0.1 mM); lane 4: DNA + **7** + NaN_3 (0.1 mM); lane 5: DNA + **7**; lane 6: DNA alone; 50 min irradiation with light of $\lambda>600$ nm. SC and NC denote supercoiled circular and nicked circular form, respectively. NC% represents the percentage of the NC form.

the photocleavage activity of **7** markedly, and this indicates a $^1O_2$ mechanism or Type II mechanism for **7**. In contrast, both NaN_3 and KI can remarkably restrict the photocleavage activity of **6** (Figure 10), which suggests that **6** exerts photodynamic activity through both Type I and Type II mechanisms. To the best of our knowledge, this is the first example that $^{\cdot}OH$ is generated on NIR irradiation of a BODIPY-type photosensitizer and participates in the damage of DNA.

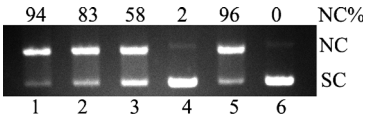

Figure 10. Comparison of agarose gel electrophoresis patterns of photocleaved supercoiled pBR322 DNA (0.1 mM in base pairs) by **6** (30 μM) in Tris/CH_3COOH/EDTA buffer (pH 7.4). Lane 1: DNA + **6** + catalase (0.05 mM); lane 2: DNA + **6** + SOD (500 U mL^{-1}); lane 3: DNA + **6** + KI (0.1 mM); lane 4: DNA + **6** + NaN_3 (0.1 mM); lane 5: DNA + **6**; lane 6: DNA alone; 50 min irradiation with the light of $\lambda>600$ nm. SC and NC denote supercoiled circular and nicked circular form, respectively. NC% represents the percentage of the NC form.

2.4. $O_2^{\cdot-}$ and $^{\cdot}OH$ Generation

Spin-trapping EPR is a powerful technique to detect formation of $O_2^{\bullet-}$ and $^{\cdot}OH$. We used DMPO as spin-trapping agent for both $O_2^{\bullet-}$ and $^{\cdot}OH$. As shown in Figure 11 b, 532 nm laser irradiation of an air-saturated acetonitrile solution of **6** or **7** and DMPO led to an EPR signal. Control experiments indicate that **6** or **7**, DMPO, irradiation, and oxygen are all necessary for appearance of this signal. We tentatively ascribe it to the signal of DMPO–$O_2^{\bullet-}$,[31] though the signal intensity is weak and the signal/noise ratio is low, probably due to the low absorptivity of **6** or **7** at the irradiation wavelength. If water is allowed into

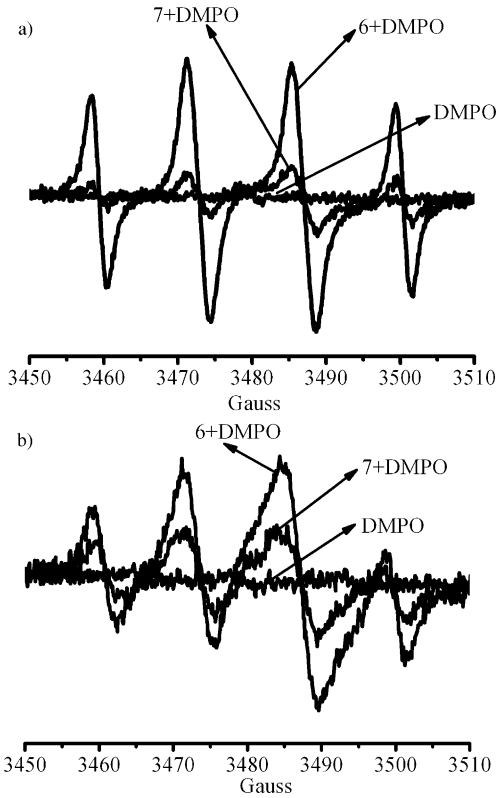

Figure 11. EPR signals obtained on irradiation of air-saturated solutions of DMPO (50 mM) and **6** or **7** (1 mM) with a 532 nm laser in acetonitrile containing 17% water (a) and in dry acetonitrile (b).

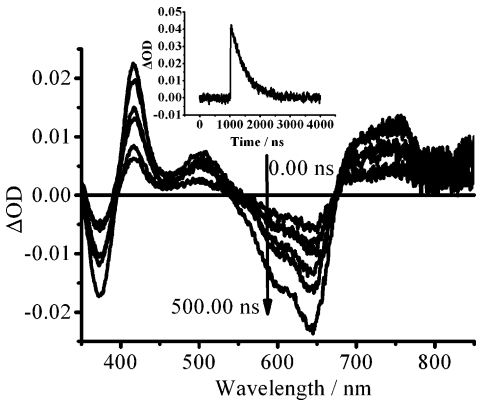

Figure 12. Transient absorption spectra of **7** following 640 nm laser pulse excitation (recorded at time delays of 0–500 ns). Inset: transient decay at 420 nm,[37] from which a triplet excited state lifetime of 475 ns was obtained by mono-exponential fitting.

the solution, irradiation causes a four-line EPR signal with intensity ratio of about 1:2:2:1 and hyperfine coupling constants of $a^N = a^H = 14.9$ G in the case of **6** (Figure 11a). Furthermore, the presence of mannitol, a well-known scavenger of $^{\bullet}OH$,[28] can inhibit signal generation (Figure S6a, Supporting Information).These results suggest the signal can be attributed to DMPO–$^{\bullet}OH$,[31] which in turn supports the assignment of EPR signal occurring in Figure 11a, because $O_2^{\bullet-}$ can transform into $^{\bullet}OH$ in aqueous solutions. Clearly, **6** sensitizes $O_2^{\bullet-}$ and $^{\bullet}OH$ more efficiently than **7**, in line with the DNA photocleavage experiments (Figures 9 and 10). We also examined $O_2^{\bullet-}$ generation sensitized by **1**–**3**. The $O_2^{\bullet-}$ generation abilities follow the order **1** > **2** > **3** (Figure S5, Supporting Information). In aqueous solution, the signal transformation from DMPO–$O_2^{\bullet-}$ to DMPO–$^{\bullet}OH$ was observed again (Figure S6, Supporting Information).

We found that O_2 has a negligible effect on the fluorescence quantum yields of the examined BODIPYs. For example, the fluorescence quantum yields of **1** in Ar- and air-saturated acetonitrile are 0.73 and 0.71, respectively. Thus, $O_2^{\bullet-}$ and $^{\bullet}OH$ generation should stem from the triplet excited state of **1**–**7**, rather than the singlet excited state.

To explore the role of the triplet excited state, the transient absorption spectra of **6** and **7** were measured. Taking **7** as an example, laser irradiation at 640 nm led to transient absorption spectra, as shown in Figure 12, from which a triplet excited state life time τ_T of 475 ns was obtained. Similarly, τ_T of **6** was measured to be 1229 ns. Both lifetimes are long enough to allow full interaction of the triplet excited states of **6** and **7** with O_2, supported by their $^1O_2$-generating abilities. As a result, τ_T is not likely the decisive factor in the generation of $O_2^{\bullet-}$ and $^{\bullet}OH$. The intersystem crossing efficiency is not the critical factor either, since **1** generates $O_2^{\bullet-}$ and $^{\bullet}OH$ most efficiently among **1**–**3**, just like the cases of **6** and **7**.

The generation of $O_2^{\bullet-}$ and $^{\bullet}OH$ must involve electron transfer; therefore, the redox potentials of **1**–**3** and **6**, **7** were measured (Supporting Information Figure S7 and Table 2). The triplet excited state energies (estimated from the phosphorescence maxima measured at 77 K) and triplet excited state oxidation potential (calculated by the subtracting the triplet excited state energy from the ground-state oxidation potential) are also included in Table 2. Clearly, electron transfer from the triplet excited states of **1**–**3** and **6**, **7** to O_2 to form $O_2^{\bullet-}$ is a thermodynamically allowed process (the redox potential of $O_2/O_2^{\bullet-}$ couple is −0.50 V vs. NHE or −0.74 V vs. SCE).[32] The more negative triplet excited state oxidation potentials of **1** (about 100 mV compared to **2** and **3**) and **6** (about 30 mV compared to **7**) may partly account for their higher $O_2^{\bullet-}$ and $^{\bullet}OH$ efficiency due to the higher driving forces for electron transfer from the excited state to O_2. Further studies on other BODIPYs are underway and will undoubtedly help to better understand the underlying mechanism for their sensitization of $O_2^{\bullet-}$ and $^{\bullet}OH$.

Table 2. Redox potentials, triplet excited state energies, and oxidation potentials of **1**–**3** and **6**, **7**.

BODIPY	E_T [eV]	E [V][b] (vs. SCE)	E [V] (vs. SCE) E_{ox}[c]	E_{red}[d]
1	2.30	−1.36	0.94	−1.15
2	2.15	−1.27	0.88	−0.91
3	2.12	−1.26	0.86	−0.93
6	1.71	−1.22	0.49	−0.28
7	1.71	−1.19	0.52	−0.29

[a] Triplet excited state energy. [b] Triplet excited state oxidation potential. [c] Oxidation peak potential. [d] Reduction peak potential.

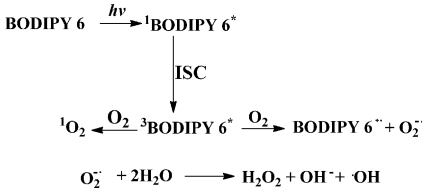

Scheme 2. Proposed DNA photodamage mechanism for BODIPY **6**.

On the basis of the above discussion, the photodynamic mechanism of **6** can be depicted as in Scheme 2. Though $O_2^{\bullet-}$ plays a role in the generation of $^{\bullet}OH$, a restricting effect of SOD and catalase on DNA photocleavage was not observed (Figure 10). This suggests that their interaction with $O_2^{\bullet-}$ can not compete with disproportionation of $O_2^{\bullet-}$ to $^{\bullet}OH$ under our experimental conditions. Our work, for first time, demonstrates that BODIPY dyes can serve as photosensitizers of not only $^1O_2$, but also $O_2^{\bullet-}$ and $^{\bullet}OH$, which may open a new structure-optimization strategy for more efficient BODIPY-based PDT agents.

3. Conclusions

New NIR-absorbing cationic BODIPY dyes **6** and **7** were synthesized, and their binding affinities and photocleavage activities toward DNA characterized in detail. It is noteworthy that **6** photocleaves DNA through both $^1O_2$ and $^{\bullet}OH$, while **7** photocleaves DNA mainly through $^1O_2$. The ability of a BODIPY dyes to generate $^1O_2$ and $^{\bullet}OH$ was demonstrated for the first time in this work, which is helpful for better understanding the BODIPY-based PDT mechanism and for further development of more efficient BODIPY-type PDT agents.

Experimental Section

Materials: 2,4-Dimethylpyrrole, 4-pyridinecarboxaldehyde, 2,3-dichloro-5,6-dicyano-1,4-benzoquinone (DDQ), boron trifluoride diethyl etherate ($BF_3{\cdot}Et_2O$, 98%), azobisisobutyronitrile (AIBN), tetra-*n*-butylammonium hexafluorophosphate, benzaldehyde, bromosuccinimide (NBS), iodomethane, and piperidine were purchased from Alfa Aesar. Catalase, ethidium bromide (EB), superoxide dismutase (SOD), sodium azide (NaN_3), mannitol, 2,2,6,6-tetramethylpiperidine (TEMP), 5,5-dimethyl-1-pyrroline-*N*-oxide (DMPO), calf thymus DNA (CT DNA), gel loading buffer, and Tris base were products of Sigma-Aldrich. The supercoiled pBR322 plasmid DNA was obtained from TaKaRa Biotechnology Company. 9,10-Anthracenediyl-bis(methylene)dimalonic acid (AMDA, $\geq$90%) was provided by Fluka. Methylene blue (MB) was a product of Beijing Chemical Works.

Spectroscopic measurements: UV/Vis absorption spectra were recorded on a Shimadzu UV-2450 spectrophotometer. Fluorescence emission spectra were run on a Hitachi F-4500 fluorescence spectrophotometer. ^1H NMR spectra were obtained on a Bruker DMX-400 spectrophotometer. High-resolution mass spectra (HRMS), EI mass spectra (EI-MS), and MALDI TOF mass spectra (MALDI TOF-MS) were determined on a Bruker Daltonics Inc. APEX II FT-ICR mass spectrometer, GCT Premier (Waters) mass spectrometer, and Microflex (Bruker) mass spectrometer, respectively. Circular dichroism (CD) spectra were recorded on a JASCO-J810 spectrometer.

The redox potentials were measured on an EG&G Model 283 Potentiostat/Galvanostat in a three-electrode cell with a platinum-wire working electrode, a platinum-plate counterelectrode, and a SCE reference electrode. Cyclic voltammetry was conducted at a scan rate of 100 $mV\,s^{-1}$ in Ar-saturated, anhydrous acetonitrile solution containing 0.1 M tetra-*n*-butylammonium hexafluorophosphate as supporting electrolyte.

The EPR spectra were taken at room temperature on a Bruker ESP-300E spectrometer at 9.8 GHz, X-band with 100 kHz field modulation. Samples were injected quantitatively into quartz capillaries and illuminated in the cavity of the EPR spectrometer with an Nd:YAG laser at 532 nm (5–6 ns pulse width, 10 Hz repetition frequency, 30 mJ/pulse energy).

Methods: All experiments involving CT DNA were performed in phosphate buffered saline (PBS, pH 7.4), unless otherwise noted. CT DNA solutions were prepared by dispersing the desired amount of DNA in buffer solution by stirring overnight at a temperature below 4 °C. The concentration of CT DNA was expressed as the concentration of nucleotides and was calculated by using the molar absorptivity of 6600 $M^{-1}\,cm^{-1}$ at 260 nm.

Measurement of $^1O_2$ quantum yield: The $^1O_2$ quantum yields of the examined BODIPYs were determined by the AMDA bleaching method, taking MB as reference whose $^1O_2$ quantum yield in aqueous solution was reported to be 0.52.[33] The photooxidation of AMDA sensitized by the examined BODIPYs was carried out by using an Oriel 91192 solar simulator as light source and a 600 nm long-pass optical filter to remove the short-wavelength light. Typically, 3 mL of BODIPY sample (ca. 5 μM, all samples were adjusted to the same optical density at 650 nm) was mixed with 100 μL of 1 mM AMDA, and then subjected to photobleaching in a standard 1 cm path length quartz cuvette. The photoreactions were followed spectrophotometrically by detecting the absorbance decrease of AMDA at 400 nm as a function of irradiation time. All samples were air-saturated and tested at room temperature.

Gel electrophoretic DNA photocleavage: DNA photocleavage abilities of the examined BODIPYs were evaluated by using supercoiled pBR322 plasmid DNA as target. A mixture of 5 μL of supercoiled pBR322 DNA (1 mM in base pairs) in PBS (pH 7.4), 5 μL BODIPY (300 μM in CH_3CN), and 40 μL PBS (pH 7.4) was irradiated under an Oriel 91192 Solar Simulator with a glass filter to cut off the light below 600 nm. After irradiation, 20 μL of gel loading buffer was added. The sample was then subjected to agarose gel (1%) electrophoresis (Tris/acetic acid/EDTA buffer, pH 8.0) at 80 V for about 1.5 h. The gel was stained with 1 $mg\,L^{-1}$ EB for 1 h, and then analyzed with a Gel Doc XR system (Bio-Rad).

n-Octanol/water partition coefficients: *n*-Octanol/water partition coefficients P_c were measured at room temperature by a reported method.[34] In brief, solutions of BODIPYs (1 mM) in equal volumes of PBS (pH 7.4, 1 mL) and *n*-octanol (1 mL) were mixed and sonicated for 30 min. After separation by centrifugation, the amounts of BODIPY in each phase were determined by measuring the absorption spectra after dilution with acetonitrile, and the results were the average of three independent measurements.

Viscosity measurements: Viscosity was measured with an Ubbelohde viscometer immersed in a constant-temperature bath at 30 °C and a stopwatch. The data were presented as $(\eta/\eta_0)^{1/3}$ versus [BODIPY]/[DNA], where η is the specific viscosity of DNA in the presence of photosensitizer and η_0 that of DNA alone in 5 mM PBS (pH 7.2). Viscosities were calculated from the observed flow time of DNA-containing solutions (t) corrected for the buffer alone (t_0): $\eta = (t-t_0)/t_0$.

EB displacement assay: Aliquots (15 μL each time) of the BODIPY or MB solution (1.0 mM in CH_3CN) were added to a 2 mL solution of EB (5 μM) and CT DNA (10 μM in base pairs) in PBS, and the mixtures allowed to stand for 15 min before fluorescence measurements. The fluorescence from EB was measured with 490 nm excitation. The apparent binding affinity K_{app} was calculated from Equation (1), where [drug] is the concentration of the BODIPY or MB at 50% reduction of EB fluorescence and K_{EB} the binding constant of EB toward CT DNA (1×10^7 M^{-1}):[35]

$$K_{EB}[EB] = K_{app}[drug] \quad (1)$$

Transient absorption and triplet excited state lifetime: Nanosecond transient absorption measurements were performed on a LP-920 laser flash photolysis setup (Edinburgh). Excitation at 640 nm with a power of 2.0 mJ/pulse from a computer-controlled Nd:YAG laser/OPO system from Opotek (Vibrant 355 II) operating at 10 Hz was directed to the sample with an optical absorbance of 0.4 at the excitation wavelength. The laser and analyzing light beam passed perpendicularly through a 1 cm quartz cell. The signals were detected by a Tektronix TDS 3012B oscilloscope and R928P photomultiplier, and finally analyzed by Edinburgh analytical software (LP920). All samples used in flash photolysis experiments were deaerated for 30 min with argon before measurements.

Synthesis: BODIPY **1** was synthesized by using the general synthetic method for BODIPY dyes.[6a] Pyrrole (230 μL, 2.25 mmol, 214 mg) and benzaldehyde (106 mg, 1.0 mmol) were dissolved in 200 mL of absolute dichloromethane under nitrogen atmosphere. Two drops of trifluoroacetic acid were added and solution was stirred at room temperature until benzaldehyde was completely consumed, monitored by TLC. Then 272 mg of DDQ (1.20 mmol) was added. After stirring for another 15 min, 5 mL of triethylamine and 5 mL of $BF_3{\cdot}Et_2O$ were added. The reaction mixture was stirred at room temperature for 2 h and washed with deionized water three times. After removal of organic solvent, the obtained solid was purified by column chromatography on silica gel (CH_2Cl_2/hexane 1/4 as eluent) to give 95 mg of **1** as a nacarat solid. Yield: 29%. ^{1}H NMR (400 MHz, $CDCl_3$): $\delta=1.37$ (s, 6H), 2.56 (s, 6H), 5.98 (s, 2H), 7.26–7.30 (m, 2H), 7.46–7.52 (m, 3H); EI-MS: *m/z* 324.16.

BODIPY **2** was prepared as follows:[12a–b] **1** (220 mg, 0.68 mmol), azoisobutyronitrile (AIBN, 223 mg, 1.36 mmol), and *N*-bromosuccinimide (NBS, 242 mg, 1.36 mmol) were heated to reflux in 15 mL of CCl_4 for 30 min. After removal of the solvent, the obtained solid was subjected to column chromatography on silica gel with CH_2Cl_2/hexane (1/5) as eluent to give 265 mg of **2** as a nacarat solid. Yield: 81%. ^{1}H NMR (400 MHz, $CDCl_3$): $\delta=1.36$ (s, 6H), 2.61 (s, 6H), 7.24–7.26 (m, 2H), 7.47–7.59 (m, 3H); EI-MS: *m/z* 481.96.

BODIPY **3** was prepared as follows:[12c–d,13] Iodic acid (232 mg, 1.32 mmol) dissolved in a 15 mL of water was added dropwise over 20 min to a solution of **1** (195 mg, 0.60 mmol) and iodine (335 mg, 1.32 mmol) in 250 mL of ethanol. The mixture was heated to reflux for 1 h. After removal of solvent, the crude product was purified by silica gel column chromatography with CH_2Cl_2/hexane (1/5) as eluent to afford 310 mg of **3** as bright red needles. Yield: 89%. ^{1}H NMR (400 MHz, $CDCl_3$): $\delta=1.38$ (s,6H), 2.65 (s, 6H), 7.21–7.25 (m, 2H), 7.49–7.56 (m, 3H); EI-MS: *m/z* 575.95.

BODIPYs **4** and **5** were synthesized as follows:[12,13] 148 mg of **2** or 177 mg of **3** (0.308 mmol), 4-pyridinecarboxaldehyde (82 mg, 0.77 mmol, 72 μL), 220 μL of glacial acetic acid, and 270 μL of piperidine in 15 mL of benzene were heated to reflux for 16 h. After removal of solvent, the crude product was purified by thin-layer chromatography on silica gel with $CHCl_3/CH_3OH$ (1/5) as eluent to give 20 mg of **4** or 110 mg of **5** as a dark green solid. Yield: 10% for **4** and 46% for **5**. BODIPY **4**: ^{1}H NMR (400 MHz, $CDCl_3$): $\delta=1.46$ (s, 6H), 7.30–7.32 (m, 2H), 7.57–7.60 (m, 7H), 7.90 (d, $J=16.7$ Hz, 2H), 8.06 (d, $J=16.7$ Hz, 2H), 8.69 (d, $J=6.0$ Hz, 4H);. MALDI-TOF MS: 658.37. BODIPY **5**: ^{1}H NMR (400 MHz, $CDCl_3$): $\delta=1.48$ (s, 6H), 7.30–7.32 (m, 2H), 7.50–7.52 (m, 4H), 7.57–7.59 (m, 3H), 7.83 (d, $J=16.7$ Hz, 2H), 8.06 (d, $J=16.7$ Hz, 2H), 8.68 (d, $J=6.0$ Hz, 4H); MALDI-TOF MS: 754.44.

BODIPYs **6** and **7** were synthesized as follows:[36] A mixture of **4** (10 mg, 0.015 mmol) or **5** (50 mg, 0.066 mmol), 10 mL of iodomethane, and 15 mL of DMF was stirred at 50 °C for 10 h. The reaction mixture was then poured into 200 mL of diethyl ether, and the precipitate collected by filtration and recrystallized from DMF to give 11 mg of **6** or 65 mg of **7** as a green solid. Yield: 77% for **6** and 95% for **7**. BODIPY **6**: ^{1}H NMR (400 MHz, [D_6]DMSO): $\delta=1.44$ (s, 6H), 4.31 (s, 6H), 7.52–7.54 (m, 2H), 7.66–7.67 (m, 3H), 7.91 (d, $J=16.7$ Hz, 2H), 8.13 (d, $J=16.5$ Hz, 2H), 8.33(d, $J=6.5$ Hz, 4H), 8.94 (d, $J=6.5$ Hz, 2H); MALDI-TOF MS: 687.41; ESI-HRMS: *m/z* calcd for $C_{33}H_{29}BBr_2F_2N_4^{2+}$: 688.0809; found: 688.0815. BODIPY **7**: ^{1}H NMR (400 MHz, [D_6]DMSO): $\delta=1.47$ (s, 6H), 4.31 (s, 6H), 7.50–7.53 (m, 2H), 7.65–7.68 (m, 3H), 7.89 (d, $J=16.7$ Hz, 2H), 8.07 (d, $J=16.5$ Hz, 2H), 8.33 (d, $J=6.5$ Hz, 4H), 8.93 (d, $J=6.5$ Hz, 2H); MALDI-TOF MS: 784.00; ESI-HRMS: *m/z* calcd for $C_{33}H_{29}BI_2F_2N_4^{2+}$: 784.0532; found: 784.0543.

Acknowledgements

This work was financially supported by NNSFC (21172228, 21101163, 20873170) and CAS (KGCX2YW-389).

Keywords: DNA cleavage · dyes/pigments · photodynamic therapy · photosensitizers · reactive oxygen species

[1] a) T. J. Dougherty, C. J. Gomer, B. W. Henderson, G. Jori, D. Kessel, M. Korbelik, J. Moan, Q. Peng, *J. Natl. Cancer Inst.* **1998**, *90*, 889–905; b) I. J. Macdonald, T. J. Dougherty, *J. Porphyrins Phthalocyanines* **2001**, *5*, 105–129; c) D. E. J. G. J. Dolmans, D. Fukumura, R. K. Jain, *Nat. Rev. Cancer.* **2003**, *3*, 380–387; d) C. A. Robertson, D. H. Evans, H. Abrahamse, *J. Photochem. Photobiol. B* **2009**, *96*, 1–8; e) J. P. Celli, B. Q. Spring, I. Rizvi, C. L. Evans, K. S. Samkoe, S. Verma, B. W. Pogue, T. Hasan, *Chem. Rev.* **2010**, *110*, 2795–2838.

[2] a) R. Bonnett, *Chem. Soc. Rev.* **1995**, *24*, 19–33; b) S. K. Pushpan, S. Venkatraman, V. G. Anand, J. Sankar, D. Parmeswaran, S. Ganesan, T. K. Chandrashekar, *Curr. Med. Chem.* **2002**, *2*, 187–207; c) M. Wainwright, *Anti-Cancer Agents Med. Chem.* **2008**, *8*, 280–291; d) J. F. Lovell, T. W. B. Liu, J. Chen, G. Zheng, *Chem. Rev.* **2010**, *110*, 2839–2857; e) M. R. Detty, S. L. Gibson, S. J. Wagner, *J. Med. Chem.* **2004**, *47*, 3897–3915.

[3] a) P. K. Frederiksen, S. P. McIlroy, C. B. Nielsen, L. Nikolajsen, E. Skovsen, M. Jørgensen, K. V. Mikkelsen, P. R. Ogilby, *J. Am. Chem. Soc.* **2005**, *127*, 255–269; b) T. Lu, P. Shao, I. Mathew, A. Sand, W. F. Sun, *J. Am. Chem. Soc.* **2008**, *130*, 15782–15783; c) M. Obata, S. Hirohara, R. Tanaka, I. Kinoshita, K. Ohkubo, S. Fukuzumi, M. Tanihara, S. Yano, *J. Med. Chem.* **2009**, *52*, 2747–2753; d) Y. Y. Huang, P. Mroz, T. Zhiyentayev, S. K. Sharma, T. Balasubramanian, C. Ruzié, M. Krayer, D. Fan, K. E. Borbas, E. Yang, H. L. Kee, C. Kirmaier, J. R. Diers, D. F. Bocian, D. Holten, J. S. Lindsey, M. R. Hamblin, *J. Med. Chem.* **2010**, *53*, 4018–4027.

[4] a) M. Wainwright, *Chem. Soc. Rev.* **1996**, *25*, 351–359; b) D. Ramaiaht, A. Joy, N. Chandrasekhar, N. V. Eldho, S. Das, M. V. George, *Photochem. Photobiol.* **1997**, *65*, 783–790; c) V. Rapozzi, L. Beverina, P. Salice, G. A. Pagani, M. Camerin, L. E. Xodo, *J. Med. Chem.* **2010**, *53*, 2188–2196.

[5] a) R. Ziessel, G. Ulrich, A. Harriman, *New. J. Chem.* **2007**, *31*, 496–501; b) A. Loudet, K. Burgess, *Chem. Rev.* **2007**, *107*, 4891–4932; c) G. Ulrich, R. Ziessel, A. Harriman, *Angew. Chem.* **2008**, *120*, 1202–1219; *Angew.*

Chem. Int. Ed. **2008**, *47*, 1184 – 1201; d) A. C. Benniston, G. Copley, H. Lemmetyinen, N. V. Tkachenko, *ChemPhysChem* **2010**, *11*, 1685 – 1692.
[6] a) W. W. Qin, M. Baruah, A. Stefan, M. Van der Auweraer, N. Boens, *ChemPhysChem* **2005**, *6*, 2343 – 2351; b) Y. Yamada, Y. Tomiyama, A. Morita, M. Ikekita, S. Aokia, *ChemBioChem* **2008**, *9*, 853 – 856; c) J. G. Wang, Y. J. Hou, C. Li, B. W. Zhang, X. S. Wang, *Sens. Actuators B* **2011**, *157*, 586 – 593; d) D. P. Wang, Y. Shiraish, T. Hirai, *Chem. Commun.* **2011**, *47*, 2673 – 2675; e) S. C. Dodani, S. C. Leary, P. A. Cobine, D. R. Winge, C. J. Chang, *J. Am. Chem. Soc.* **2011**, *133*, 8606 – 8616; f) N. Boens, W. Qin, M. Baruah, W. M. D. Borggraeve, A. Filarowski, N. Smisdom, M. Ameloot, L. Crovetto, E. M. Talavera, J. M. Alvarez-Pez, *Chem. Eur. J.* **2011**, *17*, 10924 – 10934.
[7] a) D. Kumaresan, R. P. Thummel, T. Bura, G. Ulrich, R. Ziessel, *Chem. Eur. J.* **2009**, *15*, 6335 – 6339; b) T. Rousseau, A. Cravino, E. Ripaud, P. Leriche, S. Rihn, A. D. Nicola, R. Ziessel, J. Roncali, *Chem. Commun.* **2010**, *46*, 5082 – 5084.
[8] R. P. Sabatini, T. M. McCormick, T. Lazarides, K. C. Wilson, R. Eisenberg, D. W. McCamant, *J. Phys. Chem. Lett.* **2011**, *2*, 223 – 227.
[9] a) J. Killoran, L. Allen, J. F. Gallagher, W. M. Gallagher, D. F. O'Shea, *Chem. Commun.* **2002**, *17*, 1862 – 1863; b) A. Gorman, J. Killoran, C. O'Shea, T. Kenna, W. M. Gallagher, D. F. O'Shea, *J. Am. Chem. Soc.* **2004**, *126*, 10619 – 10631; c) W. M. Gallagher, L. T. Allen, C. O'Shea, T. Kenna, M. Hall, A. Gorman, J. Killoran, D. F. O'Shea, *Br. J. Cancer* **2005**, *92*, 1702 – 1710; d) A. Byrne, W. M. Gallagher, D. F. O'Shea, *J. Am. Chem. Soc.* **2005**, *127*, 16360 – 16311; e) A. T. Byrne, A. E. O'Connor, M. Hall, J. Murtagh, K. O'Neill, K. M. Curran, K. Mongrain, J. A. Rousseau, R. Lecomte, S. McGee, J. J. Callanan, D. F. O'Shea, W. M. Gallagher, *Br. J. Cancer* **2009**, *101*, 1565 – 1573.
[10] N. Adarsh, R. R. Avirah, D. Ramaiah, *Org. Lett.* **2010**, *12*, 5720 – 5723.
[11] T. Yogo, Y. Urano, Y. Ishitsuka, F. Maniwa, T. Nagano, *J. Am. Chem. Soc.* **2005**, *127*, 12162 – 12163.
[12] a) Z. Dost, S. Atilgan, E. U. Akkaya, *Tetrahedron* **2006**, *62*, 8484 – 8488; b) S. Atilgan, Z. Ekmekci, A. L. Dogan, D. Guc, E. U. Akkaya, *Chem. Commun.* **2006**, *42*, 4398 – 4400; c) S. Erbas, A. Gorgulu, M. Kocakusakogullari, E. U. Akkaya, *Chem. Commun.* **2009**, *33*, 4956 – 4958; d) S. Ozlem, E. U. Akkaya, *J. Am. Chem. Soc.* **2009**, *131*, 48 – 49.
[13] a) H. He, P. C. Lo, S. L. Yeung, W. P. Fong, D. K. P. Ng, *J. Med. Chem.* **2011**, *54*, 3097 – 3102; b) H. He, P. C. Lo, S. L. Yeung, W. P. Fong, D. K. P. Ng, *Chem. Commun.* **2011**, *47*, 4748 – 4750.
[14] S. G. Awuah, J. Polreis, V. Biradar, Y. You, *Org. Lett.* **2011**, *13*, 3884 – 3887.
[15] P. R. Ogilby, *Chem. Soc. Rev.* **2010**, *39*, 3181 – 3209.
[16] a) J. W. Hofman, F. Zeeland, S. Turker, H. Talsma, S. A. G. Lambrechts, D. V. Sakharov, W. E. Hennink, C. F. Nostrum, *J. Med. Chem.* **2007**, *50*, 1485 – 1494; b) K. Kawai, Y. Osakada, M. Fujitsuka, T. Majima, *J. Phys. Chem. B* **2007**, *111*, 2322 – 2326; c) A. Ikeda, Y. Doi, M. Hashizume, J. Kikuchi, T. Konishi, *J. Am. Chem. Soc.* **2007**, *129*, 4140 – 4141.
[17] a) G. Viola, F. Dall'Acqua, N. Gabellini, S. Moro, D. Vedaldi, H. Ihmels, *ChemBioChem* **2002**, *3*, 550 – 558; b) P. Wang, L. G. Ren, H. P. He, F. Liang, X. Zhou, Z. Tan, *ChemBioChem* **2006**, *7*, 1155 – 1159; c) Q. X. Zhou, W. H. Lei, Y. Sun, J. R. Chen, C. Li, Y. J. Hou, X. S. Wang, B. W. Zhang, *Inorg. Chem.* **2010**, *49*, 4729 – 4731; d) Y. Sun, Y. J. Hou, Q. X. Zhou, W. H. Lei, J. R. Chen, X. S. Wang, B. W. Zhang, *Inorg. Chem.* **2010**, *49*, 10108 – 10116.
[18] D. O. Frimannsson, M. Grossi, J. Murtagh, F. Paradisi, D. F. O'Shea, *J. Med. Chem.* **2010**, *53*, 7337 – 7343.
[19] a) J. N. Demasa, G. A. Crosby, *J. Phys. Chem.* **1971**, *75*, 991 – 1024; b) D. P. Kennedy, C. M. Kormos, S. C. Burdette, *J. Am. Chem. Soc.* **2009**, *131*, 8578 – 8536.
[20] J. Olmsted, *J. Phys. Chem.* **1979**, *83*, 2581 – 2584.
[21] M. Kępczyński, R. P. Pandian, K. M. Smith, B. Ehrenberg, *Photochem. Photobiol.* **2002**, *76*, 127 – 134.
[22] N. A. Kuznetsova, N. S. Gretsova, O. A. Yuzhakova, V. M. Negrimovskii, O. L. Kaliya, E. A. Luk'yanets, *Russ. J. Gen. Chem.* **2001**, *71*, 36 – 41.
[23] a) Y. Lion, M. Delmelle, A. Vorst, *Nature* **1976**, *263*, 442 – 443; b) J. Moan, E. Wold, *Nature* **1979**, *279*, 450 – 451.
[24] a) A. M. Pyle, J. P. Rehmann, R. Meshoyrer, C. V. Kumar, N. J. Turro, J. K. Barton, *J. Am. Chem. Soc.* **1989**, *111*, 3051 – 3058; <**lit** b>D. S. Raja, N. S. P. Bhuvanesh, K. Natarajan, *Inorg. Chem.* **2011**, *50*, 12852 – 12866.
[25] a) R. Lyng, T. Härd, B. Norden, *Biopolymers* **1987**, *26*, 1327 – 1345; b) S. Allenmark, *Chirality* **2003**, *15*, 409 – 422; c) N. C. Garbett, P. A. Ragazzon, J. B. Chaires, *Nat. Protoc.* **2007**, *2*, 3166 – 3172.
[26] a) S. Mahadevan, M. Palaniandavar, *Inorg. Chem.* **1998**, *37*, 693 – 700; b) S. Mahadevan, M. Palaniandavar, *Inorg. Chem.* **1998**, *37*, 3927 – 3934; c) R. W. Y. Sun, C. K. L. Li, D. L. Ma, J. J. Yan, C. N. Lok, C. H. Leung, N. Zhu, C. M. Che, *Chem. Eur. J.* **2010**, *16*, 3097 – 3113.
[27] R. Rohs, H. Sklenar, R. Lavery, B. Roder, *J. Am. Chem. Soc.* **2000**, *122*, 2860 – 2866.
[28] S. Mettath, B. R. Munson, R. K. Pandey, *Bioconjugate Chem.* **1999**, *10*, 94 – 102.
[29] Y. Sun, Y. J. Hou, Q. X. Zhou, J. R. Chen, B. W. Zhang, X. S. Wang, *J. Inorg. Biochem.* **2011**, *105*, 978 – 984.
[30] S. Hirayama, R. Ueda, K. Sugata, *Energy. Convers. Mgmt.* **1995**, *36*, 685 – 688..
[31] a) J. R. Harbour, M. L. Hair, *J. Phys. Chem.* **1978**, *82*, 1397 – 1399; b) S. J. Xu, X. X. Zhang, S. Chen, M. H. Zhang, T. Shen, *Photochem. Photobiol. Sci.* **2003**, *2*, 871 – 876.
[32] a) D. T. Sawyer, *Acc. Chem. Res.* **1981**, *14*, 393 – 400; b) V. V. Pavlishchuk, A. W. Addison, *Inorg. Chim. Acta* **2000**, *298*, 97 – 102.
[33] a) J. M. Fernandez, M. D. Bilgin, L. I. Grossweiner, *J. Photochem. Photobiol. B* **1997**, *37*, 131 – 140; b) R. W. Redmond, J. N. Gamlin, *Photochem. Photobiol.* **1999**, *70*, 391 – 475.
[34] S. J. Wagner, A. Skripchenkol, D. Robinenel, J. W. Foley, L. Cincotta, *Photochem. Photobiol.* **1998**, *67*, 343 – 349.
[35] M. Lee, A. L. Rhodes, M. D. Wyatt, S. Forrow, J. A. Hartley, *Biochemistry* **1993**, *32*, 4237 – 4245.
[36] a) P. Hambright, E. B. FleischerL, *Inorg. Chem.* **1970**, *9*, 1757 – 1761; b) P. Hambright, T. Gore, M. Burton, *Inorg. Chem.* **1976**, *15*, 2314 – 2315.
[37] a) S. Mula, K. Elliott, A. Harriman, R. Ziessel, *J. Phys. Chem. A* **2010**, *114*, 10515 – 10522; b) J. Y. Liu, M. E. El-Khouly, S. Fukuzumi, D. K. P. Ng, *Chem. Asian J.* **2011**, *6*, 174 – 179.

Received: March 15, 2012
Published online on ■■ ■■, 2012

*J. G. Wang, Y. J. Hou, W. H. Lei, Q. X. Zhou, C. Li, B. W. Zhang, X. S. Wang**

■■ – ■■

DNA Photocleavage by a Cationic BODIPY Dye through Both Singlet Oxygen and Hydroxyl Radical: New Insight into the Photodynamic Mechanism of BODIPYs

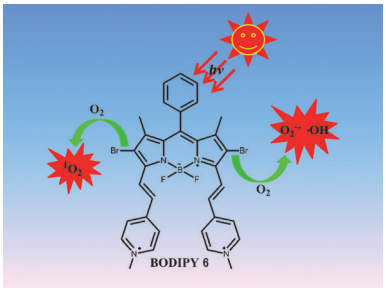

New photocleavage mechanism: New cationic BODIPY dye **6** is found, for the first time, to be able to generate singlet oxygen ($^1O_2$), superoxide anion radical ($O_2^{\bullet-}$) and hydroxyl radical ($^{\bullet}OH$) simultaneously on irradiation ($\lambda \geq 600$ nm). Both $^1O_2$ and $^{\bullet}OH$ participate in photocleavage of DNA by this BODIPY dye.

